2018

Thermodynamic Design of a Mesoscale Vapor Compression Cooling Device

Ricardo Yee
Federal University of Parana, Brazil, ricardo.yee@hotmail.com

Christian Hermes
POLO Labs, Federal University of Santa Catarina, Brazil, hermes@polo.ufsc.br

Thermodynamic Design of a Mesoscale Vapor Compression Cooling Device

Ricardo P. YEE [1], Christian J. L. HERMES [2,*]

[1] Post-Graduation Program in Mechanical Engineering, Federal University of Paraná
81531-990, Curitiba, PR, Brazil

[2] POLO Research Laboratories, Department of Mechanical Engineering, Federal University of Santa Catarina
88040-900, Florianópolis, SC, Brazil

[*] Corresponding Author: hermes@polo.ufsc.br

ABSTRACT

This paper presents a thermodynamic methodology for designing a vapor compression refrigeration system aiming at electronics cooling. A cycle simulation model was developed firstly assuming isentropic compression and isenthalpic expansion, whereas the heat exchangers (condenser and evaporator) were modelled following a distributed approach. Whilst a 3-D heat conduction model calculates the heat leakage from the condenser to the evaporator, 2-D heat conduction models provide the temperature distribution (and the heat transfer rates) at the cold and hot ends. The fluid flow was modelled as 1-D considering both the momentum and the energy conservation equations to design the heat exchangers geometry and circuitry considering the heat and fluid flow trade-offs that take place when the system is scaled down. Subsequently, semi-empirical sub-models for variable-speed compressors and fixed-orifice expansion devices were incorporated to the cycle simulation model, which was then used to assess the effect of the components characteristics (expansion orifice size, compressor stroke and speed) on the system COP. When the case where a 5×5 cm heat source at 40°C with the surroundings at 25°C is considered, the optimal design provides a cooling capacity of 110 W with a COP of 1.6. If compared to a thermoelectric device available on the market operating at the same conditions, the thermoelectric cooler provided a COP of 0.3, nearly 5 times lower than that provided by vapor compression system designed by means of the thermodynamic methods presented in this work.

1. INTRODUCTION

Because of the irreversible Joule heating, electronic computing is always accompanied by temperature raising. In modern computers, a key source of heat is the processor chip, which must be maintained within a certain temperature range to ensure a proper performance. As this technology evolves, higher processing capabilities have been observed, demanding more efficient ways to remove the generated amount of heat. Due to their simplicity, air cooled heat sinks have been the most common choice for such applications, albeit their performances are limited not only by the low temperature differences but also by the mild heat transfer coefficients typical of gaseous media when compared to vapor compression cycles where phase-change takes place (Mongia *et al.*, 2006).

At a first glance, thermoelectrical cells might be considered as an alternative, as they can be easily scaled down to fit the geometric constraints of personal computing applications, the so-called mesoscale (i.e., "*in the range of tenths of a millimeter to tenths of a meter*", as elucidated by Warren *et al.* 1999), although their intrinsic low thermodynamic efficiency (mainly because of the Joule heating) can lead to prohibitive demands for power input. Vapor compression refrigeration systems, on the other hand, are usually designed to operate in the macroscale, presenting thermodynamic efficiencies much higher than those typical of thermoelectric coolers (Hermes and Barbosa, 2012).

Miniaturization of vapor compression systems, nonetheless, is an engineering undertaking which requires a great care because of two competing phenomena: the heat transfer enhancement and the pressure drop increase as the system is downscaled (Bejan, 1987). On thermodynamic grounds, such a trade-off suggests the existence of an optimal size (scale) in which the system performance is maximized. Some believe that, for the vapor compression cycle, such an optimum takes place in the mesoscale (Phelan *et al.*, 2004).

Notwithstanding many studies concerning micro and mesoscopic vapor compression systems, from numerical simulations (Chiriac and Chiriac, 2007) to prototype construction (Nnanna, 2006; Taijong *et al.*, 2014), just a few assessed the heat and fluid flow trade-offs that take place when the system is scaled down (Sangkwon, 2004), most of them neglecting the impact of the assembly aspects on the system performance. A summary of some key works devoted to analyzing and developing cooling devices to operate in the mesoscale is presented in Table 1.

Table 1: Summary of key studies of mesoscale vapor compression cooling devices

Author	Type	Application	Capacity [W]	COP	T_{evap} [ºC]	T_{cond} [ºC]	Compressor	Condenser	Expansion	Evaporator
Chow *et al.* (1999)	Prototype	Personal cooling	32	3.34	12	60	Linear	Microchannel	Orifice	Microchannel
Shannon *et al.* (1999)	Numerical Prototype	Personal cooling	3	4-6	20	50	Diaphragm	Microchannel	Orifice	Microchannel
Heydari (2002)	Numerical model	Performance computing	170	3	20	60	Linear	Compact	Captube	Plate
Phelan *et al.* (2004)	Numerical model	High-end microelectronics	100-300	-	5	55	Scroll	Microchannel	-	-
Coggins *et al.* (2006)	Prototype	Performance computing	100	-	-70	57.4	Recip	No info	Captube	Microchannel
Mongia *et al.* (2006)	Prototype	Notebook	50	2.25	50	90	Recip	Microchannel	Needle valve	Microchannel
Nnanna (2006)	Prototype	Performance computing	152-606	1.2	4	68	Scroll	Compact	TXV	Plate
Chiriac e Chiriac (2007)	Numerical model	High-end microelectronics	100	4.24	10	55	Scroll	Microchannel	Captube	Microchannel
Wu e Du (2010)	Numerical Prototype	Microelectronics	200	5.7-7	20	45	Rotating	Microchannel	Captube	Plate
Tayde *et al.* (2013)	Numerical Prototype	Microelectronics	300	1.6	16	50	Recip	Microchannel	Captube	Microchannel
Taijong *et al.* (2014)	Prototype	-	80	2.15	-	-	Rotating	Compact	Orifice	Microchannel
Weixing *et al.* (2015)	Numerical Prototype	Small refrigerator	260	1.62	-	-	Rotating	Microchannel	TXV	Microchannel

To fill this gap, this paper introduces a thermodynamic approach for designing a mesoscopic vapor compression refrigeration system aimed at electronics cooling. The assemble considered in the present work is depicted in Fig. 1. A roll-bond, plate-type evaporator is mounted on the top of the processor chip, whose area is fixed at 5×5 cm^2 to comply with the size constraint of most thermoelectric cells available on the market. An air-supplied louvered fin-and-plate multi-layered condenser in mounted on the opposite side, whilst an insulating material is sandwiched between the condenser and the evaporator to mitigate the crossed heat transfer leakage. The expansion is provided by a fixed orifice. Both the compressor and the condenser fan are placed out of the array.

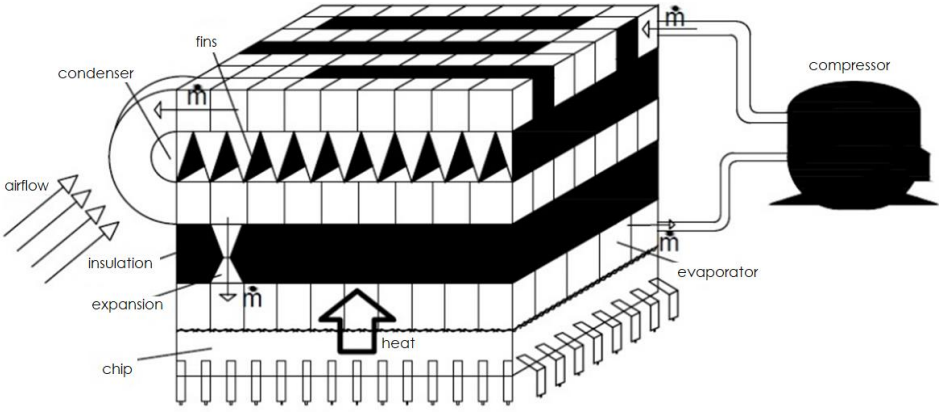

Figure 1: Schematic view of the mesoscale vapor compression cooling device considered in this study

Refrigerant R134a – whose lower scale threshold is $D_h \approx La = 1.02$ mm, where $La \cong (\sigma/g\rho_l)^{1/2}$ is the Laplace number (Serizawa *et al.*, 2002) – was selected as the working fluid. Other reasons for doing so rely on the availability of two-phase flow correlations and compressor data for such a working fluid, albeit higher critical-point refrigerants like isobutane (R600a) might perform better than R134a in such applications.

2. SIMULATION MODEL

To comply with the area and volume constraints, the evaporator and the condenser circuitry must be designed not only aiming at the maximum heat transfer rates, but also at minimum heat leakage to provide a thin insulation thickness between the hot and cold ends. For doing so, a cycle simulation model was firstly developed assuming isentropic compression and isenthalpic expansion, whereas the heat exchangers (condenser and evaporator) were treated as multidimensional. The fluid flow was modelled according to a 1-D distributed approach, considering both the momentum and energy conservation equations to assess the fluid and heat flow trade-offs that take place when the system is scaled down. A 3-D heat conduction model calculates the heat leakage from the condenser to the evaporator, whereas 2-D heat conduction models provide the temperature distribution (and the heat transfer rates) at the cold and hot ends. Semi-empirical sub-models for variable-speed compressors and fixed-orifice expansion devices were subsequently included in the cycle simulation model, which was then used to assess the effect of the components characteristics (compressor stroke and speed, expansion orifice size) on the system COP.

2.1 Refrigeration Loop

The cycle simulation model requires sub-models for each of system components illustrated in Fig. 1. Invoking the energy conservation and applying the fundamental principles of heat transfer to the evaporator and condenser, yields

$$Q_{evap} = m\left(i_6 - i_5\right) = UA_{evap}\left(T_{chip} - T_{evap}\right) \tag{1}$$

$$Q_{cond} = m\left(i_2 - i_3\right) = UA_{cond}\left(T_{cond} - T_{amb}\right) \tag{2}$$

where the indices 2, 3, 5 and 6 stand for the condenser inlet, condenser outlet, evaporator inlet and evaporator outlet, respectively, and m is the refrigerant mass flow rate in [kg/s]. Also, the power consumption in a real compression can be split into two terms – namely, the heat lost to the environment and the enthalpy delivered to the fluid,

$$W_{comp} = Q_{comp} + m(i_2 - i_1) \tag{3}$$

where the index 1 stands for compressor inlet. The expansion process in a fixed orifice was taken as isenthalpic, i.e., $i_4 = i_5$, where the index 4 stands for outlet of the liquid line. The temperature at the compressor inlet, on the other hand, was calculated considering the possibility of using an internal heat exchanger between the liquid and the suction line, as follows

$$T_1 = T_6 + \varepsilon(T_3 - T_6) \tag{4}$$

where ε is the heat exchanger effectiveness, whereas the liquid line outlet enthalpy is calculated from $i_4 = i_3 - i_1 + i_6$. The closing equations required for computing the working (condensing, evaporating) pressures usually come from the refrigerant charge inventory and the continuity of the mass flow rate, i.e., the rate of mass discharged by the compressor must be equal to the one flowing through the expansion device. The solution of such set of equations is likely to bring about convergence issues because of the nonlinear dependence of the working pressures. A pragmatic solution relies on imposing the superheating and subcooling degrees at the heat exchangers outlets, thus reducing the nonlinear 2×2 equation set to a straightforward calculation. In this work, zero superheating and subcooling degrees have been considered to comply with the best practices of keeping the evaporator fully activated, and the amount of refrigerant minimal, respectively, in such a way that $p_{evap} = p_{sat}(T_6)$ and $p_{cond} = p_{sat}(T_3)$.

2.2 Heat Exchangers

The heat exchangers were both considered as roll-bond, plate-type. Due to the innumerous degrees of freedom for the refrigerant circuitry design, three of the most common configurations in micro and macroscopic systems were considered, namely (a) standard, (b) nested and (c) parallel, all illustrated in Fig. 2. The overall heat transfer model is

represented by the array of thermal resistances depicted in Fig. 3a, according to which the UA-coefficients for both the condenser and the evaporator were calculated. The refrigerant flow was solved by considering unidimensional nonoverlapping control volumes of length δ, as illustrated in Fig. 3b, to which the principles of momentum and energy conservation have been respectively applied, yielding

$$[p] + G[u] + \tfrac{1}{8}\bar{f}G\bar{u}\,P\delta/A = 0 \tag{5}$$

$$G\left[i + \tfrac{1}{2}u^2\right] \pm \bar{q}\,P\delta/A = 0 \tag{6}$$

where $[\phi]=\phi_k-\phi_{k-1}$ stands for the difference between the ϕ-values available at the outlet (k) and at the inlet (k-1) of the k-th control volume (Hermes *et al.*, 2008), whereas the overhead bar indicates the arithmetic mean, $(\phi_k+\phi_{k-1})/2$. The symbol (±) must be replaced by (+) for the evaporator and (–) for the condenser.

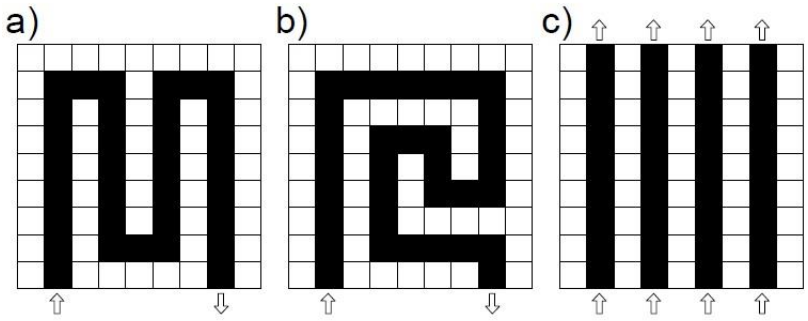

Figure 2: Schematic view of some prospective heat exchangers circuitries: (a) standard; (b) nested; and (c) parallel

The temperatures on the plate in control-volumes in direct contact with the refrigerant circuitry were assumed to be equal to the evaporating temperature. The temperature field on the rest of the plate, i.e. control-volumes not in direct contact with the refrigerant circuitry, was obtained from a two-dimensional heat diffusion formulation (see Fig. 3c), which combines the energy conversion principle with the Fourier law, yielding the following difference equation for a typical control-volume of the discretized domain (i,j):

$$k\left(T_{i+1,j} + T_{i-1,j} - 2T_{i,j}\right)w\Delta y/\delta x^2 + k\left(T_{i,j+1} + T_{i,j-1} - 2T_{i,j}\right)w\,\Delta x/\delta y^2 + (q_{ext} + q_{ins})\Delta x\Delta y = 0 \tag{7}$$

where k is the thermal conductivity of the plate material with thickness w, whereas q_{ext} and q_{ins} are, respectively, the heat fluxes from the air to the plate and from it to the insulating material sandwiched between the condenser and the evaporator. Equation (7) was solved by means of a finite-volume approach following closely the methodology introduced by Hermes *et al.* (2008).

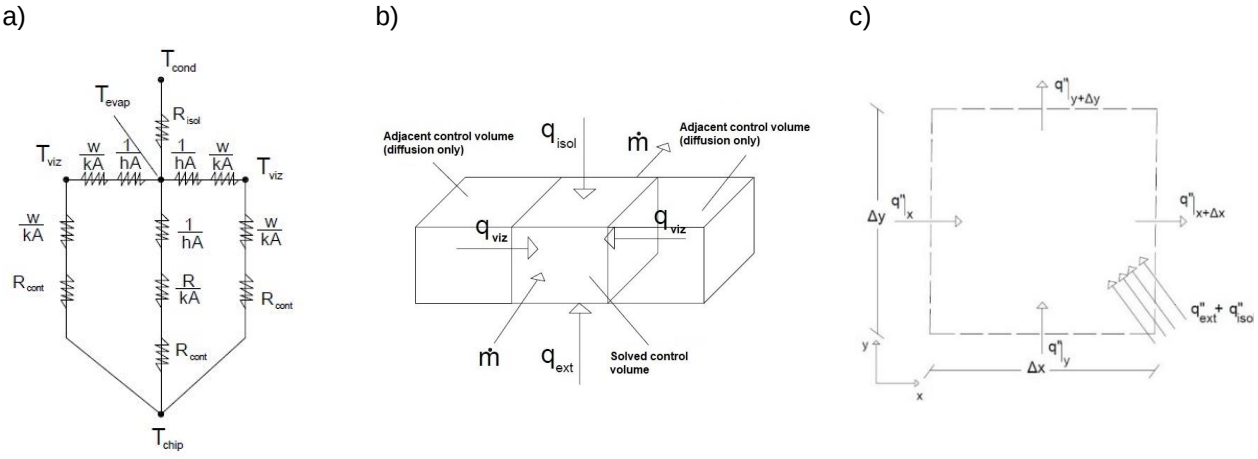

Figure 3: Overall thermal model (a), and typical control volumes for the refrigerant (b) and heat flow (c)

The air-side heat transfer coefficient of the multi-layered condenser was calculated by the Kim and Bullard (2002) correlation for louvered fins, while the chip-evaporator interface was modelled as a contact resistance between silicon and aluminum bound by a 0.02-mm layer of epoxy (Peterson *et al.*, 1987). The correlation proposed by Kim and Mudawar (2014) was used to determine the pressure loss during condensation, while the correlation of Cavallini *et al.* (2006) was used for the condensing heat transfer coefficient. The pressure drop and the heat transfer coefficient for evaporating refrigerant were calculated by the Sempértegui-Tapia (2016) correlations, whose results are compared to the experimental data (obtained from the same author) in Fig. 4.

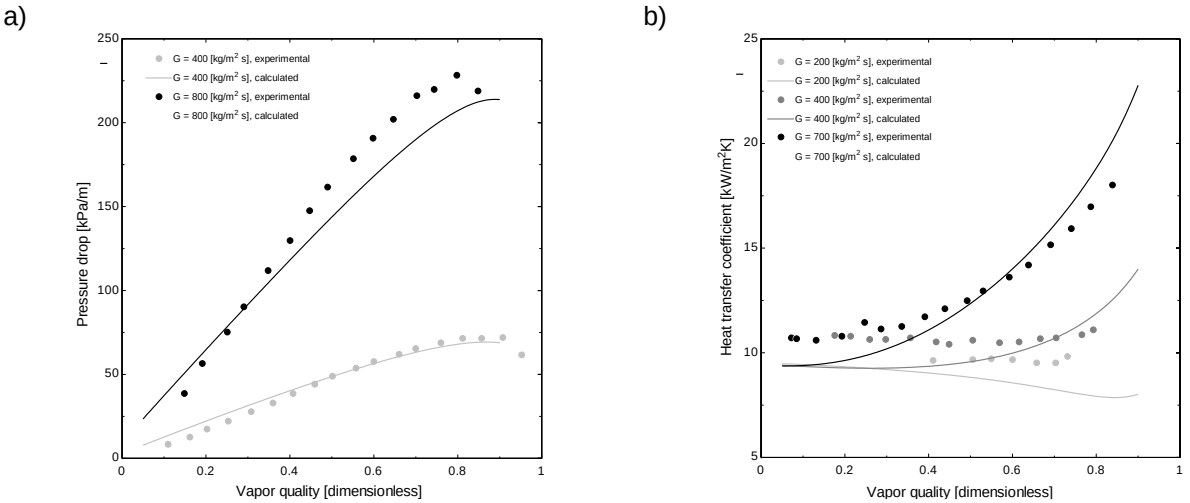

Figure 4: Evaporation model according to Sempértegui-Tapia (2016): (a) pressure drop; (b) heat transfer coefficient

2.3 Expansion Device

A fixed-orifice was considered as the expansion device, being modelled according to the following orifice equation:

$$\dot{m} = \frac{C_D}{\sqrt{1-\left(A_5/A_4\right)^2}} A_5 \sqrt{2\left(\frac{p_{cond}-p_{evap}}{v_4}\right)} \tag{8}$$

where C_D is the discharge coefficient of the orifice, v_4 is the specific volume at the inlet of the expansion device, whereas $A_5=\pi D^2/4$ is the cross-sectional area at the exit port of the orifice.

2.4 Reciprocating Compressor

The volumetric efficiency of the compressor can be defined as $\eta_v=\dot{m}v_1/VN$, where v_1 is the specific volume of refrigerant at the suction port, the product VN is the piston-displacement in [m^3/s] and $\dot{m}$ is the mass flow rate in [kg/s]. Similarly, the overall compression efficiency is defined as $\eta_g=\dot{m}w_s/W_{comp}$, where w_s is the specific isentropic work. Therefore, the rate of heat transferred through the compressor shell can be calculated from $Q_{comp}=(1-\eta_g)W_{comp}$, while the compression power was calculated as follows:

$$W_{comp} = p_{evap} VN \frac{\eta_v}{\eta_g} \frac{\gamma}{1-\gamma}\left[\left(p_{cond}/p_{evap}\right)^{1-1/\gamma}-1\right] \tag{9}$$

Rigola *et al.* (2005) evaluated the compression efficiencies for various compression chamber aspect ratios, concluding that they sharply approach zero as the aspect ratio becomes smaller. Such an observation was retrieved in the present work to scaling down the compressor, not only because the dead volume would occupy a large fraction of the compression chamber as it gets smaller, but also because of the increasing refrigerant leakage through the valves. Since there is no data available in the open literature for compressors operating in the mesoscale, manufacturer's data for the volumetric and overall efficiencies of regular, 60-Hz single-speed reciprocating compressors were taken at the same pressure ratio of the mesoscale system under analysis (≈2.8). The data was fitted

as a function of the compressor stroke using an empirical (rational equation) model which drives the efficiencies to zero for very small compressor strokes, V, as illustrated in Fig. 5.

Additionally, a way to compensate the volumetric flow losses as the compressor volume gets smaller consists in raising the speed, so that this variable must also be accounted for by the model. A judicious analysis of the experimental data for various compressor speeds available from the market for two compressors with 10.0 and 14.3 cm^3 stroke, as depicted in Fig. 6, reveals that the volumetric and overall efficiencies presented the same trends for both compressors, being independent of the stroke. Therefore, correction factors based on the experimental fits of the data points in Fig. 6 were included in the rational equation models to take the speed into account. The resulting empirical equations for volumetric and overall compressor efficiencies are respectively as follows,

$$\eta_v = \left[\frac{-0.000492 + 1.291V}{1 + 1.614V + 0.0337V^2}\right] - 5.5\cdot10^{-5}(N - 3600) \tag{10}$$

$$\eta_g = \left[\frac{-0.00298 + 3.044V}{1 + 3.234V + 0.0787V^2}\right] - \left[6\cdot10^{-5} + 2.5\cdot10^{-8}(N - 3600)\right](N - 3600) \tag{11}$$

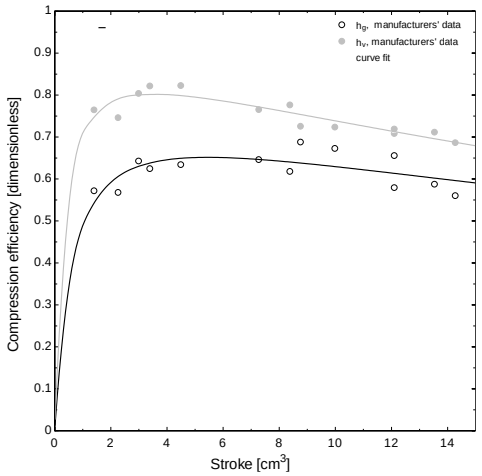

Figure 5: Curve fittings of volumetric and overall efficiencies as a function of the compressor stroke

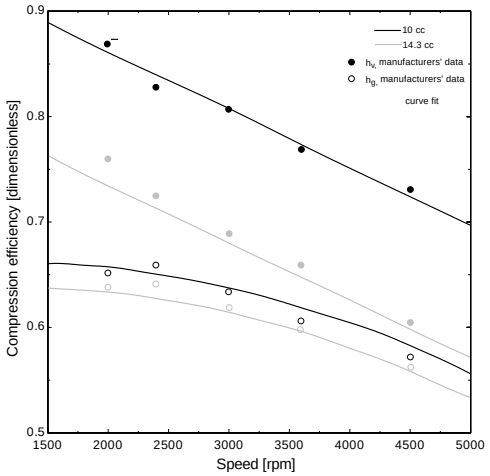

Figure 6: Curve fittings of volumetric and overall efficiencies as a function of the compressor speed

2.5 Solution Algorithm

The solution algorithm consists of two sequential iterative loops, one for the refrigeration cycle (Eqs. 1-4) and another for the heat diffusion on the heat exchanger walls (Eqs. 5-7), placed within a third (external) iterative loop where the heat conduction through the insulation layer is solved and the heat exchange between the refrigerant and the outer side (air, chip) of the heat exchanger is converged (Yee, 2017). The model was coded in `SCILAB` where the thermodynamic properties of the refrigerant were obtained from `REFPROP`. In all cases, convergence was assumed when all the differences between the current and previous iteration were within the ±0.1% thresholds.

3. DISCUSSION

Firstly, the effect of the heat exchangers circuitry was analyzed. At this stage, isentropic compression and isenthalpic expansion were considered, with zero sub-cooling and zero superheating at the condenser and evaporator outlets, respectively. The processor chip was kept at 40°C with the surrounding environment at 25°C. Figure 7 shows the COP (normalized in relation to the highest value achieved in the optimization exercise) as a function of the hydraulic diameter of the evaporator. One can notice that the system COP improves as the cross-section of the refrigerant flow in the evaporator becomes smaller, which is due to the heat transfer intensification for small characteristic lengths. However, when considering circuitries with a single channel (e.g., standard and nested arrangements in Fig. 2a and 2b), the pressure drops raise significantly for small bore channels, in such a way that an optimal COP is observed for $D_h \approx 1.4$ mm, which is not noticed for the parallel configuration (see Fig. 2c).

Despite presenting relatively small gains in terms of COP in comparison to the other configurations, the parallel arrangement experiences a performance increase throughout the whole mesoscale region, being the best choice (albeit some practical issues related to refrigerant maldistribution might take place). The parallel configuration results in a lower average evaporating temperature, due to the reduced pressure drops, while also maintaining a higher suction pressure, when compared to the single channel configurations, as depicted in Fig. 8. Henceforth, it was assumed that D_h=1.02 mm – the Laplace number for R134a, therefore the smallest dimension considered.

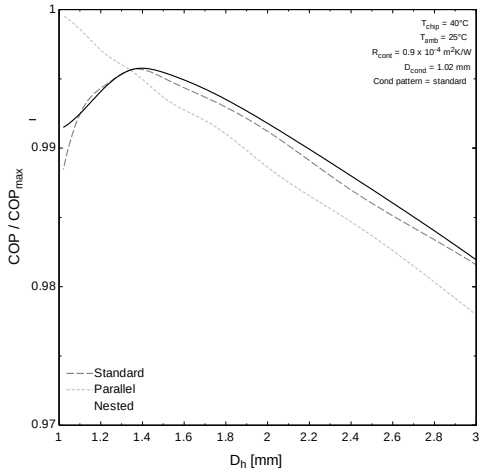

Figure 7: Variation of the COP as a function of the evaporator characteristic length

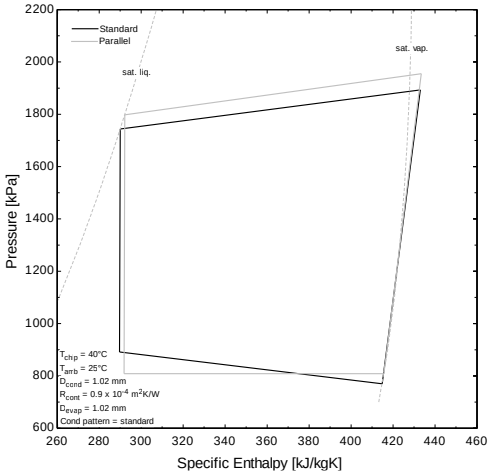

Figure 8: Representation of the refrigeration cycle in a p-h diagram for different evaporator configurations

The temperature distributions on the evaporator surface are depicted in Fig. 9. One can see that the standard and nested configurations have non-uniform temperature distributions, with a significant temperature decrease along the channel despite of the increasing vapor quality of refrigerant. This can be easily explained by the increased pressure drops for long length configurations, particularly for bores as small as 1 mm, as the channel is filled with two-phase refrigerant. The parallel configuration, on the other hand, presented a nearly uniform temperature distribution, favoring the heat transfer from the chip to the cooling device.

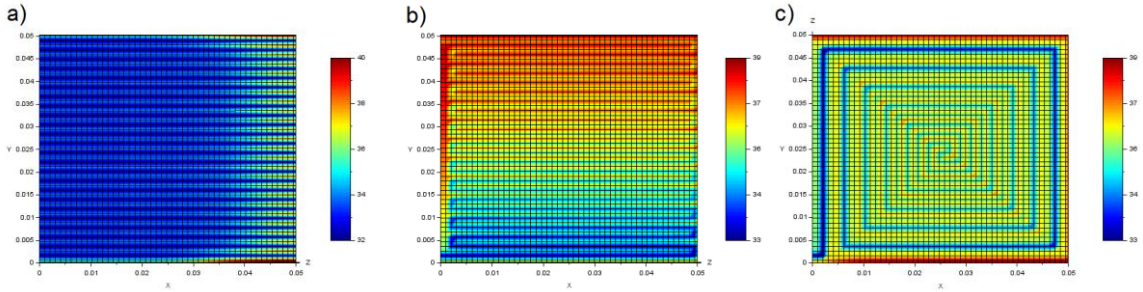

Figure 9: Temperature field for multiple heat exchanger circuitries: (a) parallel; (b) standard; and (c) nested

On the condenser side, one can see in Fig. 10 that the standard configuration with 1.11 mm presented slightly better results than the nested configuration. When compared to the evaporator, such results can be explained by the higher pressure and specific mass, mitigating the pressure loss effect in favor of the heat transfer enhancement for small bore channels. It is noticeable the decrease in the condensing pressure while the evaporating pressure experienced no practical changes when small bore channels were used in comparison to large ones, which in turn reduce the heat transfer coefficient, thus increasing the condensing pressure to prohibitive levels, as depicted in Fig. 11.

The internal heat exchanger between the liquid and the suction line was also assessed, as depicted in Fig. 12, where COP_0 refers to a cycle with no internal heat exchanger, i.e. ε=0. One can see that the system COP decreases as the effectiveness increases, as the condensing pressure raises whereas the evaporating pressure remains nearly the same, as illustrated in Fig. 13. Additional analyses were conducted to investigate the effect of the insulation layer and the orifice size, coming up with a 10-mm thick PU insulation – such that the loss in system performance was not as impactful, while trying to maintain a relatively small envelope – and 0.26 mm diameter (Yee, 2017).

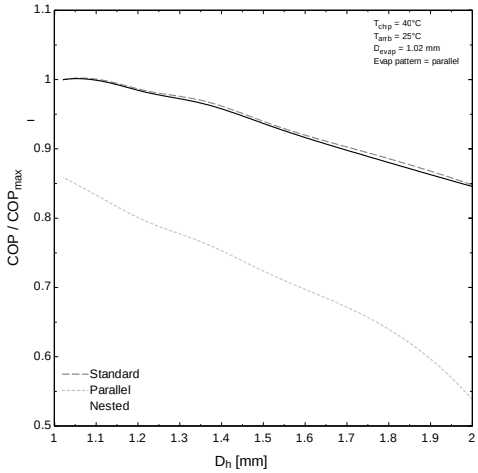

Figure 10: Variation of the COP as a function of the condenser characteristic length

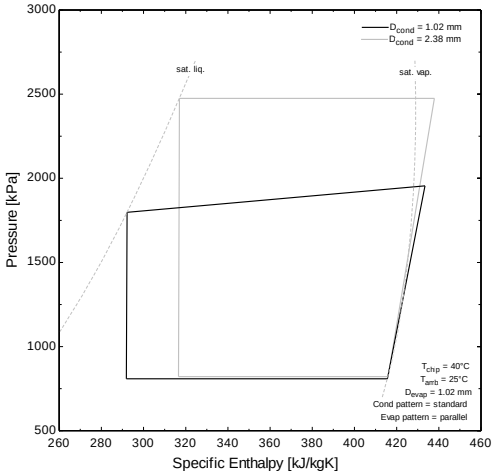

Figure 11: Representation of the refrigeration cycle in a p-h diagram for different condenser configurations

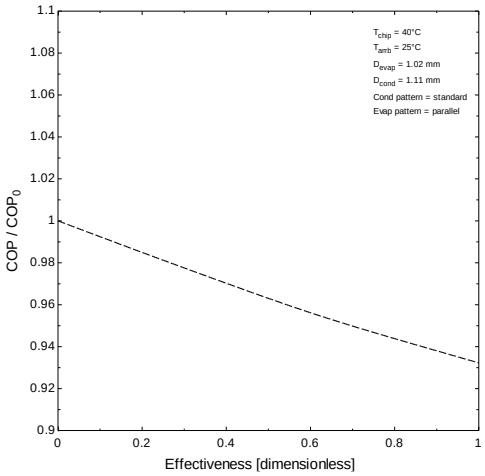

Figure 12: Variation of the COP/COP_0 as a function of the effectiveness and the insulation thickness

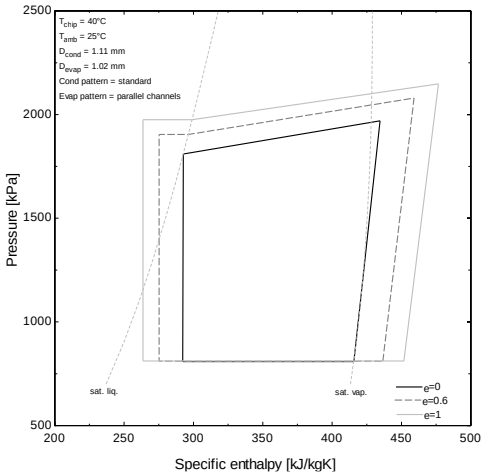

Figure 13: Representation of the refrigeration cycle in a p-h diagram for different heat exchanger effectiveness

Finally, the analysis considering a real compression process suggests that increasing the compressor speed may be not an effective way to compensate the capacity reduction resulted from compressor stroke downsizing. This is so because of the significantly lower efficiencies for higher speeds, causing an increase in the cooling capacity but only within a limited range, as illustrated in Fig. 14. It is clear from Fig. 14 that each compressor stroke is applicable to a different range of speeds, thus existing a maximum cooling capacity for each pair stroke/speed.

Figure 15 shows the system COP evaluated for the conditions of maximum cooling capacity as a function of the compressor stroke. Higher COPs are observed for the smaller strokes, albeit the system must be able to remove a minimum amount of heat to maintain the electronic component at a certain temperature. It was established a limit of 100 W, such that the smallest volume considered was of 0.75 cc. A compressor with 1.2 cc presented the maximum $COP/COP_{int,rev}$ ratio – where $COP_{int,rev}$ stands for the coefficient of performance of an internally reversible refrigerator operating between two reservoirs at the condensing and evaporating temperatures – providing 115 W at 2675 rpm, whereas the 0.75 cc compressor provided 100 W at 3300 rpm with a $COP/COP_{int,rev}$ ratio by 7% lower.

For the sake of comparisons, it is worth noting that these two configurations outperformed the thermoelectric cell technology, which provide a COP of 0.31 and a cooling capacity of 101 W for $T_{hot}–T_{cold}\approx40$ K (Chein and Huang, 2004). In addition, considering a simple fan-cooled heat sink mounted directly over the chip surface, which has a thermal resistance by 0.24 K/W (Mouser, 2017), for $T_{chip}–T_{amb}\approx15$ K the heat transfer rate can be estimated at 62 W, a figure ~40% lower than that achieved by means of the mesoscale cooling device.

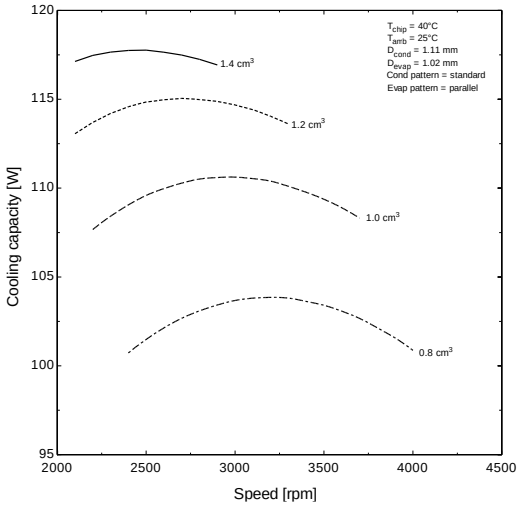

Figure 14: Cooling capacity as a function of the compressor speed and stroke

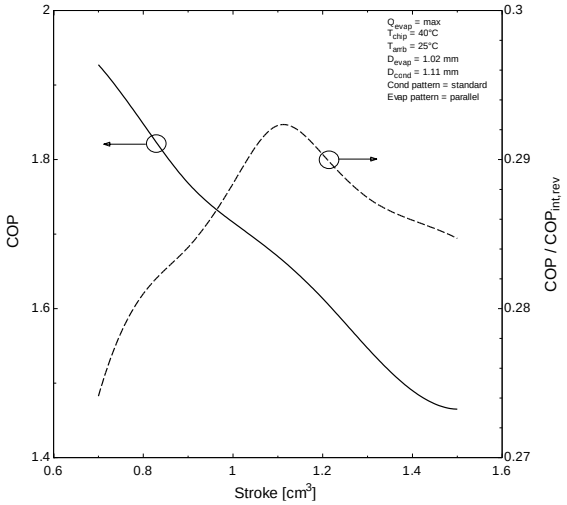

Figure 15: System COP and efficiency as a function of compressor stroke for maximum cooling capacity

4. FINAL REMARKS

In this study, design guidelines were proposed for component sizing and matching for a mesoscale vapor compression system aiming at electronics cooling applications. The scaling effects were perceived and evaluated for each of the system components, enabling a proper design of the refrigerant circuitry and flow area for the heat exchangers and, to some extent, the compressor sizing. The simulation results confirmed the existence of an optimal component size within the mesoscale which is due to the competing heat transfer and pressure drop effects. In addition, the analysis of the manufacturer's data has shown the difficulty experienced by reciprocating compressors in maintaining high efficiencies for small strokes and high speeds, resulting in a cooling capacity threshold when the vapor compression system is downsized. Nevertheless, the proposed system presented a cooling capacity of up to 110 W, with COP figures ranging from 1.5 to 1.9. When compared to existing technologies available for the same scale, the proposed design succeeded in intensifying the cooling capacity across a large temperature difference in size-restrained, electronics cooling conditions.

NOMENCLATURE

Roman

A	Cross-sectional area, m^2
COP	Coefficient of Performance, dimensionless
D	Diameter, m
D_h	Hydraulic diameter, m
f	Darcy friction factor, dimensionless
G	Mass flux, kg $m^{-2}s^{-1}$
h	Heat transfer coefficient, W/m^2K
i	Specific enthalpy, kJ kg^{-1}
m	Mass flow rate, kg s^{-1}
N	Compressor speed, Hz
N	Compressor speed, s^{-1}
p	Pressure, Pa
q	Heat flux, W m^{-2}
Q	Heat transfer rate, W
T	Temperature, K
u	Flow velocity, m/s
UA	Thermal conductance, W K^{-1}
V	Compressor stroke, m^3
W	Power consumption, W

Greek

ε	Effectiveness, dimensionless
γ	Isentropic exponent, dimensionless
η_v	Volumetric efficiency, dimensionless
η_g	Overall efficiency, dimensionless
ρ	Density, kg/m^3

Subscripts

1…6	Position along the refrigeration loop
amb	Surroundings
chip	Processor chip
comp	Compressor
cond	Condenser
evap	Evaporator
ext	External
ins	Insulation
liq	Liquid refrigerant
sat	Saturation
vap	Vapor refrigerant

REFERENCES

Bejan A (1987) The thermodynamic design of heat and mass transfer processes and devices, *Heat & Fluid Flow* 8, 258-276

Cavallini A, Del Col D, Doretti L, Matkovic M, Rosseto L, Zilio C (2006) Condensation in Horizontal Smooth Tubes: a New Heat Transfer Model for Heat Exchanger Design, *Heat Transfer Eng.* 27, 31-38

Chein R, Huang G (2004) Thermoelectric cooler application in electronic cooling, *Appl. Therm. Eng.* 24, 2207-2217

Chiriac F, Chiriac V (2007) An Alternative Method for the Cooling of Power Microelectronics Using Classical Refrigeration, *Thermal Issues in Emerging Technologies*

Chow LC, Carter III HC, Kapat JS, Aveau A, Sundaram KB, Vaidya J (1999) Component Fabrication and Testing for a Meso-Scale Refrigerator, *AIAA* 99-4154

Coggins C, Gerlach D, Joshi Y, Fedorov A (2000) Compact, Low Temperature Refrigeration of Microprocessors, *Int. Refrigeration and Air Conditioning Conference*, paper 814

Hermes CJL, Barbosa JR (2012) Thermodynamic Comparison of Peltier, Stirling, and Vapor Compression Portable Coolers, *Applied Energy* 91, 51-58

Hermes CJL, Melo C, Negrão COR (2008) A numerical simulation model for plate-type, roll-bond evaporators, *Int. J. Refrig.* 31, 335-347

Heydari A (2002) Miniature Vapor Compression Refrigeration System for Active Cooling of High Performance Computers, *Thermal and Thermomechanical Phenomena in Electronic Systems*, 371–378

Kim M, Bullard CW (2002) Air-Side Thermal Hydraulic Performance of Multi-Louvered Fin Aluminum Heat Exchangers. *Int. J. Refrig.* 25, 390-400

Kim S-M, Mudawar I (2014) Review of Databases and Predictive Methods for Pressure Drop in Adiabatic, Condensing and Boiling Mini/Micro-Channel Flows, *Int. J. Heat Mass Transfer* 77, 74-97

Mongia R, Masahiro K, Distefano E (2006) Small Scale Refrigeration System for Electronics Cooling within a Notebook Computer, *Thermal and Thermomechanical Phenomena in Electronics Systems*, 751-758

Mouser (2017) Product Specifications, *https://www.mouser.com/Thermal-Management/Heat-Sinks/_/N-5gg0*

Nnanna AGA (2006) Application of Refrigeration System in Electronics Cooling, *Appl. Therm. Eng.* 26, 18–27

Peterson GP, Fletcher LS (1987) Thermal Contact Resistance of Silicon Chip Bonding Materials, *Int. Symp. Cooling Technology for Electronic Equipment*, 438-448

Phelan PE, Swanson J, Chiriac F, Chiriac V (2004) Designing a Mesoscale Vapor-Compression Refrigerator for Cooling High-Power Microelectronics, *Thermal and Thermomechanical Phenomena in Electronic Systems*

Rigola J, Pérez-Segarra CD, Laboratori AO (2005) Parametric Studies on Hermetic Reciprocating Compressors, *Int. J. Refrig.* 28, 253-266

Sangwon J (2004) How difficult is it to make a micro refrigerator?, *Int. J. Refrig.* 27, 309-313

Sempértegui-Tapia DF (2016) *Experimental analysis of the effect of cross-sectional geometry and the performance of low GWP fluids on convective boiling in reduced-size channels*, PhD dissertation, University of São Paulo, São Carlos - SP, Brazil (in Portuguese)

Serizawa A, Feng Z, Kawara Z (2002) Two-Phase Flow in Microchannels, *Exp. Therm. Fluid Sci.* 26, 703-714

Shannon MA, Philpott ML, Miller NR, Bullard CW, Beebe DJ, Jacobi A, Hrnjak PS, Saif T, Aluru N, Sehitoglu H, Rockett A (1999) Economy J, Integrated Mesoscopic Cooler Circuits, *ASME-AES* 39, 75-82

Taijiong S, Donghun L, Hwa Soo K, Jongwon K (2014) Development of a Novel Meso-Scale Vapor Compression Refrigeration System (mVCRS), *Appl. Therm. Eng.* 66, 453-463

Tayde MM, Bhuyar LB, Thakre SB (2013) Design and Development of Mini-Scale Refrigerator, Am. Int. J. Research in Science, Technology, *Engineering & Mathematics* 13, 163-168

Warren WL, Dubois LH, Wax SG, Gardos MN, Fehrenbacher LL (1999) Mesoscale Machines and Electronics: There's Plenty of Room in the Middle, *ASME-AES* 39, 3-8

Weixing Y, Bo Y, Yufei Y, Kexian R, Jian X, Yibing L (2015) Development and Experimental Study of the Characteristics of a Prototype Miniature Vapor Compression Refrigerator, *Appl. Energy* 143 47-57

Wu Z, Du R (2011) Design and Experimental Study of a Miniature Vapor Compression Refrigeration System for Electronics Cooling, *Appl. Therm. Eng.* 31, 385-390

Yee RP (2017) *Application of vapor compression refrigeration system in the mesoscale: A thermodynamic analysis*, MEng thesis, Federal University of Parana, Curitiba - PR, Brazil (in Portuguese)

ACKNOWLEDGEMENTS

Financial support from the Brazilian Government funding agencies CAPES and CNPq is duly acknowledged.